Joint Centre for Mesoscale Meteorology, Reading, UK

A Preliminary Study of Fourier Series Analysis for Cloud Tracking with GOES High Temporal Resolution Images

Z. Wang

Internal Report No. 79

October 1997

Met Office Joint Centre for Mesoscale Meteorology Department of Meteorology
University of Reading PO Box 243 Reading RG6 6BB United Kingdom
Tel: +44 (0)118 931 8425 Fax: +44 (0)118 931 8791
www.metoffice.com

Designed and produced by the Met Office © Crown copyright 2001 01/0240 The Met Office logo is a registered trademark.

A Preliminary Study of Fourier Series Analysis for Cloud Tracking with GOES High Temporal Resolution Images

Z. WANG*
University of Reading

Submitted to
Journal of Applied Meteorology

October 1997

* Permanent address: Department of Atmospheric Physics, Nanjing Institute of Meteorology, Nanjing, Jiangsu 210044, P.R.C.

A Preliminary Study of Fourier Series Analysis for Cloud Tracking with GOES High Temporal Resolution Images

Z. WANG*
University of Reading, UK

ABSTRACT Fourier series analysis is proposed as a new technique for deriving cloud motion winds from high temporal resolution satellite images. Based on the change of harmonic phase, the Fourier technique computes phase speed as an estimate of cloud motion. A speed spectrum is also derived, the standard deviation of which might provide information on speed difference of clouds in different scales in an analysed area if contribution from noise could be removed. A practical example shows the ability to obtain more extensive and detailed cloud motion winds from high temporal resolution images with the Fourier method than from traditional 30-minute interval images with maximum correlation technique. It also reveals problems of noisy wind fields that require further investigation before the Fourier technique can be regarded as a viable technique.

KEY WORDS: Fourier Series, Cloud Motion Winds, GOES High Temporal Resolution Images

1. Introduction

Sequential images with a temporal resolution of one minute or even less can be obtained from the new generation of GOES satellite(Menzel and Purdom, 1994). Thus the number of the cloud motion winds(CMW) is expected to be improved because of the increase in the number of useful tracers resulting from short-lived cumulus over both water and land(Shenk, 1991). Purdom(1996) showed that the availability of imagery at such high frequencies is valuable for deriving mesoscale fields of motion. However, the spatial resolution of 4km for the infrared(IR) images is large compared with the distance typically travelled by a cloud in one minute, and a problem of estimating sub-pixel motion arises when conventional methods are used to extract cloud motions from these high temporal resolution images. The result is that wind vectors in the cloud motion wind field fluctuate very much.

* Corresponding author: Department of Atmospheric Physics, Nanjing Institute of Meteorology, Nanjing, Jiangsu 210044, P.R.C.

G. Garrett Campbell and James F. W. Purdom(personal communication) in addressing this problem, are understood to have successfully developed a technique using a quadratic function to fit a 2-dimensional distribution of correlation coefficients, derived from a conventional CMW procedure based on the maximum correlation matching technique(Kidder and Vonder Haar, 1995). This enables the positioning of the maximum in the matching surface to be found analytically so that a better estimate of the correct alignment between two templates than the maximum correlation coefficient. In the present paper, another, rather different technique, using Fourier series analysis, is introduced to address the problem of sub-pixel motion. Additional information, such as the velocity spectrum discussed below in Section 4, can also be computed with this technique. New problems arise associated with the application of this technique and interpretation of the results and they remain to be resolved. The purpose of this short paper is to introduce the new approach, to indicate its potential and to reveal the difficulties, so that other researchers might be able to contribute to their resolution.

2. Theoretical analysis of Fourier series technique

2-1. A monofrequency image line — an idealized situation

Suppose the image intensity along a particular line in the direction of the x-axis is expressed by a periodic cosine function, as shown in Fig.1,

$$I(x,t) = I_0 + I_1 \cos\varphi(x,t) \tag{1}$$

where

$$\varphi(x,t) = G(x) - H(t) \tag{2}$$

is the phase, from which the following parameters are determined:

angular wave number $K = \frac{d\varphi}{dx} = \frac{dG(x)}{dx}$ (3)

wave length $\lambda = 2\pi / K$ (4)

angular frequency $\omega = -\frac{d\varphi}{dt} = \frac{dH}{dt}$ (5)

frequency $\upsilon = 2\pi / \omega$

phase speed $u = \frac{dx}{dt} = \frac{\omega}{K} = \frac{dH}{dt} / \frac{dG}{dx}$ (6)

At x=0, G(0)=0, and $\varphi(0,t) = -H(t)$ is the original phase at x=0 at time t.

Fig.1 Schematic of an image line

Suppose also that the change in intensity determined by I_0 and I_1 from t_1 to t_1+dt is negligible, so that u can be estimated by comparing two images with a time interval dt around $x=0$. The phase speed u is taken as the rate of travel of the feature at position x, i.e., the speed of cloud motion.

Take a part of this image line around $x=0$. Let $M=2L$ be the length taken (Fig. 1). Only this part is used to estimate u around $x=0$. Then the image intensity inside the range $[-L, L]$ can be expanded as a Fourier series as follows:

$$I(x,t)=\frac{a_0}{2}+\sum_{n=1}^{\infty}(a_n\cos\frac{n\pi x}{L}+b_n\sin\frac{n\pi x}{L})$$
$$=\frac{a_0}{2}+\sum_{n=1}^{\infty}c_n\cos(\frac{n\pi x}{L}-h_n) \qquad (7)$$

where

$$a_n=\frac{1}{L}\int_{-L}^{L}I(x,t)\cos\frac{n\pi x}{L}dx\,,\ \text{n=0,1,2,}\cdots\cdots$$

$$b_n=\frac{1}{L}\int_{-L}^{L}I(x,t)\sin\frac{n\pi x}{L}dx\,,\ \text{n= 1,2,3,}\cdots\cdots \qquad (8)$$

$$c_n=\sqrt{a_n^2+b_n^2}\,,$$

$$h_n=arc\,tg(\frac{b_n}{a_n}) \qquad (9)$$

If c_n is independent of time, the phase speed for the n-th harmonic in Eq.7 would be

$$u_n=\frac{L}{n\pi}\frac{dh_n}{dt} \qquad (10)$$

However, coefficients a_n, b_n, c_n and h_n are generally a function of time. The question is " Is u_n a good estimate of u ? ".

For the simple situation given,

$$G(x)=\frac{2\pi x}{\lambda} \qquad (11)$$

then

$$u=\frac{\lambda}{2\pi}\frac{dH}{dt} \qquad (12)$$

and the suitability of u_n as an estimate of u depends on the ratio of M to λ, the variation of c_n during the time period from t_1 to $t_1 + dt$, and the value of $H(t)$ in this period.

If M, the length of the image line taken for Fourier analysis, is equal to λ (the length of the wave in image intensity function), then, u_1 (the phase speed of the first harmonic, which is the only harmonic in this simple example) is exactly the same as u (see A-1 in Appendix). If M is an integral number of wavelength, say m times, then u can be worked out exactly by Fourier analysis for u_m (the phase speed of the m-th harmonic, which is the only harmonic in this simple example) (see A-2 in Appendix). Such a result is only theoritically true. Noise from image sampling and numerical computing is a natural cause which results in a spurious spectrum from Fourier analysis.

Taking into account that the fact that the wavelength is possibly uncertain in practice and that the ratio, $r = M / \lambda$ can be any real value, then simply increasing M improves the stability of c_n (see Eq.A16 in Appendix) and further the estimate of the speed by computing the amplitude-weighted average of phase speed over all u_n in a spectrum from Fourier analysis (see Eq.A18 in Appendix).

If $r < 1$, the statistical characteristics of phase speeds from Fourier analysis are influenced by the value of $H(t)$ and the temporal variation of c_n in the period $[t_1, t_1 + dt]$. If $H(t)$ is not small enough to make $\frac{1 + Q_n^2 tg^2 H}{1 + tg^2 H} \approx 1$ in Eq.A6, a better estimate of the travelling speed from the n-th harmonic should be

$$\hat{u}_n = u_n \frac{1 + Q_n^2 tg^2 H}{1 + tg^2 H} \tag{13}$$

The factor, $\frac{1 + Q_n^2 tg^2 H}{1 + tg^2 H}$, is 1 when $H(t)$ is either 0 or π, and takes its maximum Q_n^2 when $H(t) = \pm\frac{\pi}{2}$. Thus, phase speed may be underestimated by as much as a factor of Q_n^2. Since this

underestimation can not be corrected in practice and is a function of n, the spread of computed u_n is made wider.

The amount of change of c_n with time depends on the value of $H(t)$ (see Eq.A15). Even though image intensity along thex-axis is monofrequency with a wavelength of λ, changes of c_n with time play a role in modulating the amplitudes of components in the Fourier expansion (see Eq.A11 for M/λ =0.5, for example). This is equivalent to an image intensity function which is composed of many frequency components (See Section 2-2). Thus the spread of u_n is widened further.

2-2. A multi-frequency image line ——— corresponding to an actual cloud image line

Rather than a monofrequency cosine function as given in Eq.1, the image intensity function along the x-axis is often a combination of a number of periodic functions according to Fourier theory,

$$I(x,t) = I_0 + \sum_k I_k \cos[G_k(x) - H_k(t)] \qquad (14)$$

where I_0 is the mean intensity, I_k is the amplitude of the k-th component, and $G_k(x) - H_k(t)$ is its phase. Each component has its own wavelength, angular frequency, original phase at x=0, and phase speed. The travelling speed of the k-th component, u_k, is separately determined by taking the term $I_k \cos[G_k(x) - H_k(t)]$ as a monofrequency image line,

$$u_k = \frac{dH_k(t)}{dt} / \frac{dG_k(x)}{dx} \qquad (15)$$

The visual speed of the image intensity function along the x-axis is estimated from an average of u_k for all the components in Eq.14, and the spectrum of u_k is a measure of the speed of clouds on different scales (expressed by different wave-lengths). This is the fourth contribution to the wide spread of phase speed resulting from Fourier analysis.

3. Further discussion about the application of the Fourier technique

From the analysis above, the principal problem in the application of the Fourier series technique to cloud tracking is related to determining the position "x=0" such that, at this position, the value of original phase $H(t)$ in the period $[t_1, t_1 + \Delta t]$ is as small as possible. The value of $H(t)$ in the time period $[t_1, t_1 + \Delta t]$ depends not only on the position of "x=0" but also on the phase speed or the angular frequency ω, and the time interval Δt. For any t in $[t_1, t_1 + \Delta t]$ at x=0, the phase is

$$H(t) = H(t_1) + \omega (t - t_1) \tag{16}$$

and the phase speed is $u = \frac{\lambda}{2\pi}\omega$. For instance, the satellite GOES-8 provides infrared images with a time resolution of 1 minute and a spatial resolution of 4km. For a cloud lump of λ =100km=25pixels travelling at a speed of u =16ms^{-1}, one has ω=0.001 s^{-1} and $\Delta H = H(t_2)$ - $H(t_1) = \omega \Delta t$ =0.06. Suppose that "x=0" has been chosen such that $H(t_1)$ =0, then $H(t_2)$ =0.06 and $\overline{tg^2 H} \approx 0.002$ on average over this time period. Provided the template size is M =16pixels=64km, then $\gamma = M/\lambda$ =0.64. Since $Q_n = \frac{n}{\gamma} = \frac{n\lambda}{M}$ =1.563n, $\frac{1 + Q_n^2 \overline{tg^2 H}}{1 + \overline{tg^2 H}} \approx 1$ even for the practical maximum of n =8. Therefore, a good estimate of cloud motion speed is expected from Fourier series analysis. Otherwise, if $H(t_1) = \pi/4$, $\frac{1 + Q_n^2 \overline{tg^2 H}}{1 + \overline{tg^2 H}} = \frac{1 + Q_n^2}{2}$, then, according to Eq.13, u_n would be 9ms^{-1} for n =1 and decreases to 0.2ms^{-1} as n increases to 8, which would lead to an underestimate of the true u.

To minimise $H(t)$ at x=0 implies that positions of local maxima or minima of intensity function should be chosen as the position for "x=0". Theoretical experiments to simulate a mass of cellular cloud at different scales and moving at different speeds have proved this, but more research is needed before this can be applied successfully to actual images. In the following section, when actual images are used as an example, this is not yet taken into account.

To make $Q_n \approx 1$, we must have $n\lambda \approx M$. Thus for a given M, λ is limited, i.e., long wave components in image intensity function have pernicious effects on speed estimation.

In Fourier series technique, velocity-folding exists in principle. Since the estimate of u from the n-th harmonic is

$$u_n = \frac{L}{n\pi}\frac{\Delta h_n}{\Delta t} \tag{37}$$

where $h_n = arc\,tg(\frac{b_n}{a_n})$. If h_n changes more than 2π, such as 2π+α, in the time period Δt, then Δh_n would be α rather than 2π+α because $tg\,(2\pi+\alpha)= tg\,\alpha$. So the estimated speed folds at

$$u_n = \pm\frac{2L}{n\Delta t} \tag{38}$$

For $M \equiv$2L=64km, Δt=64sec, $u_1 = \pm 1000 ms^{-1}$ and $u_8 = \pm 125 ms^{-1}$. Therefore, folding rarely happens.

4. An example of cloud tracking by means of Fourier series analysis

Satellite images obtained from a rapid scan sequence of GOES-8 images were sliced into many rectangular templates, each of which has a size of M in x-direction by N in y-direction. Each template of cloud is tracked in both x- and y-directions. Because images are expressed by discrete pixels, M is in units of pixels and N is in units of lines when the objective is to calculate latitudinal component of cloud motion, whereas M is in units of lines and N is in units of pixels when the objective is to calculate longitudinal component. Fourier series is analysed for each line, and an amplitude-weighted average over all the phase speeds and a standard deviation with respect to the average are worked out for each template of interest. The spectrum of phase speeds of all lines in a template is a measure of variation in horizontal speed.

Figure 2 is an example of the application of the Fourier technique to actual images. Figure 2a is the GOES-8 IR image taken at 14:41:36 on 5 February 1997 in the area of 37°N—57°N and 23°W—50°W. It is one in a sequence of rapid-scan images obtained during one of the Intensive Observing Periods during the Fronts and Atlantic Storm Track Experiment(FASTEX) (Joly et al. 1997). The sub-areas in the top-left and bottom-right corners are blank because of the limited area over which the rapid-scan sequence could be obtained. Figure 2b is the cloud motion vectors derived with the Fourier technique from a triplet of IR images taken at 14:40:32, 14:41:36 (as shown in Fig.2a), and 14:42:40. As a compromise between the stability of c_n and the computing efficiency, $M = N$=22 was taken as the template size for Fourier analysis. The size is between the typical values

of 16×16(Kidder and Vonder Haar, 1995) and 32×32(Buhler and Holmlund, 1993). Figures 2c gives the standard deviation associated with the vectors in Fig.2b. For a visual comparison, Figure 2d gives the CMW fields derived from 30-minute GOES-8 IR images observed at 14:15:15, 14:45:13 and 15:15:15 with the technique based on maximum-cross-correlation (Wang et al, 1997).

better definition.

Fig.2 An example of cloud motion winds. (a) GOES-8 IR image observed at 14:41:36 on 5 Feb. 1997. (b) CMW field derived from GOES-8 one-minute interval IR images observed around 14:41:36 on 5 Feb. 1997 with Fourier technique. (c) Phase speed standard deviation associated with (b). The method to present standard deviation is that the amplitude in the x-direction is the standard deviation in u-component and the amplitude in the y-direction is the standard deviation in v-component. (d) CMW field derived from GOES-8 thirty-minute interval IR images observed around 14:45:13 on 5 Feb. 1997 with traditional maximum-cross-correlation technique. ◿ = 20m s^{-1}, └ = 4m s^{-1}, └ =2m s^{-1}.

Each quadrant of the image area in Fig.2a has its own distinctive cloud features. The two quadrants on the left are covered by lumpy, cellular clouds, though the cloud in the top-left quadrant is generally higher than that in the bottom-left quadrant. Most of the rectangular templates in these two quadrants are suitable for tracking with the Fourier technique and the CMW field(Fig.2b) in this area has therefore a fairly good regular pattern. In the top-right quadrant, widely spread, high clouds with low and middle clouds underneath are dominant. They are not good for tracking because of lack of texture. In the bottom-right, the multi-layered cloud structure is more easily seen because the high cloud in this area is broken into a few long, narrow bands on the right running from south-west to north-east and massive lumps constituting a long, wide band on the left. As discussed in the last section, difficulties which are associated with the Fourier technique and lead to underestimation of CMW would appear more likely in this area. Underestimation of phase speed for any one of the two wind components would make the CMW fields noisy in both wind speed and direction, as is shown by the irregular pattern of CMWs on the right in Fig.2b.

Compared with the CMW field in Fig.2d, the field in Fig.2b is quite reasonable in the two quadrants on the left, and the general flow pattern of cloud motions toward north-east in the two quadrants on the right is also reflected. Figure 2b shows more local variabilities of cloud motion than Fig.2d does. This difference is partly because of the capability for obtaining extra CMW estimates using the rapid scan data used and partly because of the noise resulting from the unsolved problems in the Fourier technique. Verification of each CMW vector needs more effort in future.

Five causes for the width of the u_n spectrum in each template have been discussed. The contributions from image sampling and numerical computing, from the temporal variation of c_n and the underestimation of u_n, are noise while the contributions from a multi-frequency image line and from all lines in an image template are information. Further research is needed to estimate their relative magnitude so that the information can be extracted from spectrum.

The standard deviation in Fig.2c is solely an expression of the spectrum width with respect to the amplitude-weighted mean (in Fig.2b). It can be seen that most of the standard deviation vectors point to the north-east. This implies that the u- and v- components have the same standard deviation. Along the back edge of the long, wide cloud band running from about 40°N, 38°W to 53°N, 33°W, the CMWs are point more nearly to the north and the standard deviation vectors show that the standard deviation of the v-component is larger than that of the u-component. The magnitude of the standard deviation in the bottom-left quadrant is generally larger than that in the top-left quadrant. A possible explanation is that the bottom-left quadrant is a diffuse area(Fig.2b). On the right side, the underestimation of phase speed is likely the main reason for the variability in standard deviation.

Quality control for the Fourier technique is another aspect which needs further research. In the CMW inferring procedure with the Fourier technique, the criterion $|u_n - \bar{u}| < 2\sigma_u$ is used to reject some of u_n's which are too far from the amplitude-weighted average $\bar{u}$ in terms of σ_u resulting from all of

the harmonics analysed. The CMW vectors and standard deviations shown in Figs.2b and 2c are those after this criterion-control is performed.

To further eliminate the influence of change of c_n with time on phase speed estimation, a criterion, $\frac{|c_n(t_1) - c_n(t_2)|}{c_n(t_1) + c_n(t_2)} \leq \delta c$, was tested for different values of δc with the expectation that the vectors given in Fig.2b can be improved if a suitable δc is used. However, the experimental results are not as expected. Smaller values of δc lead to less components available for computing the weighted average of phase speeds and poorer consistency of CMW field in horizontal. Though a larger M is helpful to alleviate the influence of the temporal variation of c_n on the tracking result, further research with more cases is needed to improve the implementation of the constraint.

A quality flag, as a quality mark for each CMW vector before any CMW field consistency analysis was performed(Wang et al, 1997), was initialised tentatively with the ratio of the number of harmonics available for computing final $\bar{u}$ to the total number of harmonics practically analysed. The more components that are rejected, the lower the quality flag attached to $\bar{u}$. Arguments against this definition exist because neglect of some components should lead to an improvement of quality of $\bar{u}$. In addition, it seems that other information such as mean brightness, amplitudes, phases and their temporal variations resulted from Fourier analysis procedure should also be taken into account for a better definition.

5. Conclusions

Fourier series analysis for deriving cloud motion winds from high temporal resolution images has been discussed. A practical example shows encouraging results. Based on the change of harmonic phases, the Fourier technique computes phase-speed spectrum, of which the mean is used as an estimate of cloud motion. The standard deviation of the speed spectrum includes both noise, which seems inherent in the technique, and information representing the speed variation of clouds at different scales and the horizontal change in the analysed area. As a new technique, it has many

problems in both theory and implementation. This is a preliminary study and much further research is needed to improve our understanding and evaluate its utility.

6. Acknowledgements

This research was carried out at the Joint Centre for Mesoscale Meteorology, University of Reading, whilst the author was in receipt of a Sino-British Friendship Scholarship.

The author gratefully acknowledges Prof. Keith Browning for his kind supervision and constant encouragement during this study and his comments to improve this paper. The author is also grateful to James Purdom, Jack Dostalek and colleagues in the Colorado State University for the provision of GOES-8 satellite data and the RAMSDIS system for image data processing. The author has benefited from discussions with Graeme Kelly in the European Centre for Medium-Range Weather Forecasts and Liu Chunlei in the University of Reading.

Particular thanks are given to JCMM and the Department of Meteorology, University of Reading, for providing the author with the research facilities used during his stay.

7. References

Buhler,Y. and Holmlund, K. 1993: The Cloud Motion Wind Extraction Algorithm for MTP/MPEF. *Proceedings to Second International Wind Workshop*, in Tokyo, Japan, 13-15 Dec. 1993, 205-217.

Joly ,A.., Jorgensen, D., Shapiro,M. A., Thorpe A. J., Bessemoulin, P., Browning, K. A., Cammas, J. P., Chalon, J. P., Clough, S. A., Emanuel, K. A., Eymard, L., Gall, R., Hildebrand, P. H., Langland, R. H., Lemaitre, Y., Lynch, P., Moore, J. A., Persson, P. O. G., Snyder, C. and Wakimoto, R. M. 1997: the Fronts and Atlantic Storm-Track Experiment(FASTEX): Scientific objectives and experimental design. *Bull. Amer. Meteor. Soc.* To appear shortly.

Kidder, S. Q. and Vonder Haar, T. H., 1995: Satellite Meteorology: An Introduction. Academic Press, p236.

Menzel, W.P. and Purdom, J. F., 1994: Introducing GOES-I: The first of a new generation of geostationary operational environmental satellites. Bull. Amer. Meteor. Soc., 75, 757-781.

Purdom, J. F. W., 1996: Detailed cloud Motions from Satellite Imagery Taken at Thirty second, One and Three Minute Intervals, Proceedings to the 3rd International Wind Workshop in Ascona, Switzerland, 10-12 June 1996, 137-146.

Shenk, W. E., 1991: Suggestions for improving the derivation of winds from geosynchronous satellites, Proceedings to the Workshop on wind Extraction from Operational Meteorological Satellite Data, in Washington D.C., 17-19 September 1991, 173-179.

Wang, Z., Browning, K. A. and Kelly, G. A., 1997: Verification of the Tracking Technique used in an Experimental Cloud Motion Wind Inferring System. Submitted to Q. J. R. M. S.

8. Appendix

Substituting Eqs. 1, 2, and 11 into Eq.8, one has

$$a_0 = \frac{1}{L}\int_{-L}^{L}\{I_0 + I_1\cos(\frac{2\pi x}{\lambda} - H(t))\}\,dx$$
$$= \frac{1}{L}\{2I_0 L + I_1\frac{\lambda}{2\pi}[\sin(\frac{2L\pi}{\lambda} - H(t)) + \sin(\frac{2L\pi}{\lambda} + H(t))]\}$$
$$= 2I_0 + \frac{\lambda I_1}{\pi L_1}\sin\frac{2\pi x}{\lambda}\cos(H(t)) \qquad \text{(A1)}$$

$$a_n = \frac{1}{L}\int_{-L}^{L}\{I_0 + I_1\cos(\frac{2\pi x}{\lambda} - H(t))\}\cos\frac{n\pi x}{L}\,dx$$

$$= \frac{I_1}{L}\int_{-L}^{L}\cos(\frac{2\pi x}{\lambda} - H(t))\cos\frac{n\pi x}{L}\,dx$$
$$= \frac{I_1}{2L}\int_{-L}^{L}\{\cos[(\frac{2\pi}{\lambda} + \frac{n\pi}{L})x - H] + \cos[(\frac{2\pi}{\lambda} - \frac{n\pi}{L})x - H]\}dx$$
$$= \frac{I_1}{2L}\{\frac{1}{\frac{2\pi}{\lambda} + \frac{n\pi}{L}}\sin[(\frac{2\pi}{\lambda} + \frac{n\pi}{L})x - H]\Big|_{-L}^{L} + \frac{1}{\frac{2\pi}{\lambda} - \frac{n\pi}{L}}\sin[(\frac{2\pi}{\lambda} - \frac{n\pi}{L})x - H]\Big|_{-L}^{L}\}$$
$$= \frac{I_1}{2L}\{\frac{2L\lambda}{2L\pi + n\lambda\pi}\sin\frac{2L\pi + n\lambda\pi}{\lambda}\cos(H) + \frac{2L\lambda}{2L\pi - n\lambda\pi}\sin\frac{2L\pi - n\lambda\pi}{\lambda}\cos(H)\}$$

$$= I_1\cos(H(t))\{\frac{\lambda}{2L\pi + n\lambda\pi}\sin\frac{2L\pi + n\lambda\pi}{\lambda} + \frac{\lambda}{2L\pi - n\lambda\pi}\sin\frac{2L\pi - n\lambda\pi}{\lambda}\} \qquad \text{(A2)}$$

$$b_n = \frac{1}{L}\int_{-L}^{L}\{I_0 + I_1\cos(\frac{2\pi x}{\lambda} - H(t))\}\sin\frac{n\pi x}{L}\,dx$$
$$= \frac{I_1}{L}\int_{-L}^{L}\cos(\frac{2\pi x}{\lambda} - H(t))\sin\frac{n\pi x}{L}\,dx$$
$$= \frac{I_1}{2L}\int_{-L}^{L}\{\sin[(\frac{2\pi}{\lambda} + \frac{n\pi}{L})x - H] - \sin[(\frac{2\pi}{\lambda} - \frac{n\pi}{L})x - H]\}dx$$
$$= \frac{I_1}{2L}\{\frac{-1}{\frac{2\pi}{\lambda} + \frac{n\pi}{L}}\cos[(\frac{2\pi}{\lambda} + \frac{n\pi}{L})x - H]\Big|_{-L}^{L} + \frac{1}{\frac{2\pi}{\lambda} - \frac{n\pi}{L}}\cos[(\frac{2\pi}{\lambda} - \frac{n\pi}{L})x - H]\Big|_{-L}^{L}\}$$
$$= \frac{I_1}{2L}\{\frac{-2L\lambda}{2L\pi + n\lambda\pi}\sin\frac{2L\pi + n\lambda\pi}{\lambda}\sin(H) + \frac{2L\lambda}{2L\pi - n\lambda\pi}\sin\frac{2L\pi - n\lambda\pi}{\lambda}\sin(H)\}$$

$$= I_1\sin(H(t))\{\frac{-\lambda}{2L\pi + n\lambda\pi}\sin\frac{2L\pi + n\lambda\pi}{\lambda} + \frac{\lambda}{2L\pi - n\lambda\pi}\sin\frac{2L\pi - n\lambda\pi}{\lambda}\} \qquad \text{(A3)}$$

and, from Eq.9,

$$tg(h_n(t)) = \frac{b_n}{a_n} = Q_n tg(H(t)) \qquad \text{(A4)}$$

where

$$Q_n = \frac{\frac{-\lambda}{2L\pi + n\lambda\pi}\sin\frac{2L\pi + n\lambda\pi}{\lambda} + \frac{\lambda}{2L\pi - n\lambda\pi}\sin\frac{2L\pi - n\lambda\pi}{\lambda}}{\frac{\lambda}{2L\pi + n\lambda\pi}\sin\frac{2L\pi + n\lambda\pi}{\lambda} + \frac{\lambda}{2L\pi - n\lambda\pi}\sin\frac{2L\pi - n\lambda\pi}{\lambda}} \qquad \text{(A5)}$$

is independent of time.

From Eq.A4,

$$\frac{dH}{dt} = \frac{1}{Q_n}\frac{1+Q_n^2 tg^2 H}{1+tg^2 H}\frac{dh_n}{dt} \qquad \text{(A6)}$$

Provided that $H(t)$ =0 at time t , then

$$\frac{dH}{dt} = \frac{1}{Q_n}\frac{dh_n}{dt} \qquad \text{(A7)}$$

Equations A6 and A7 show the theoretical relationship between $\frac{dH}{dt}$ and $\frac{dh_n}{dt}$. Since we usually do not know $H(t)$ and Q_n in practice, the case 'Q_n=1' would be beneficial for speed estimation.

A-1. An ideal case

M ≡2L=λ , i.e., a complete wave around x=0 is taken for Fourier analysis(see Fig.1). Then

$$a_0 = 2I_0$$

$$a_n = \begin{cases} 0, & n \neq 1 \\ I_1 \cos(H(t)), & n = 1 \end{cases}$$

$$b_n = \begin{cases} 0, & n \neq 1 \\ I_1 \sin(H(t)), & n = 1 \end{cases}$$

$$c_n = \begin{cases} 0, & n \neq 1 \\ I_1, & n = 1 \end{cases} \qquad h_n = \begin{cases} 0, & n \neq 1 \\ H(t), & n = 1 \end{cases}$$

Substituting these into Eq.7, one has

$$I(x,t) = I_0 + I_1 \cos(\frac{\pi x}{L} - h_1)$$

Since c_n is independent of time and $g_1(x) = \frac{\pi x}{L}$, from Eq.10, one has

$$u_1 = \frac{L}{\pi}\frac{dh_1}{dt} = \frac{\lambda}{2\pi}\frac{dH}{dt}$$

This implies that the estimated speed from Fourier coefficients a_1 and b_1 is exactly the same as the true speed in Eq.12. It can be shown from Eq.A5 that this is the case 'Q_1=1'.

A-2. Another ideal case

M≡2L =mλ, m = any integers, i.e., the range taken for Fourier analysis includes many complete waves. Then

$$a_0 = 2I_0$$

$$a_n = \begin{cases} 0, n \neq m \\ I_1 \cos(H(t)), n = m \end{cases}$$

$$b_n = \begin{cases} 0, & n \neq m \\ I_1 \sin(H(t)), & n = m \end{cases}$$

$$c_n = \begin{cases} 0, & n \neq m \\ I_1, & n = m \end{cases}, \qquad h_n = \begin{cases} 0, & n \neq m \\ H(t), & n = m \end{cases}$$

Substituting these into Eq.7, one has

$$I(x,t) = I_0 + I_1 \cos(\frac{m\pi x}{L} - h_m)$$

Since c_m is independent of time, from Eq.10 one has

$$u_m = \frac{L}{m\pi}\frac{dh_m}{dt} = \frac{\lambda}{2\pi}\frac{dH}{dt} \qquad \text{(A8)}$$

This implies that the estimated speed from non-zero Fourier coefficients a_m and b_m is exactly the same as the true speed in Eq.12. It can be shown from Eq.A5 that this is the case 'Q_m=1'.

A-3. M≡2L=λ/2

In this case, the range [-L,L] is quite narrow and only a half wave in Fig.1 is taken. From Eqs.A1-A6,

$$a_0 = 2I_0 + \frac{4I_1}{\pi}\cos(H(t))$$

$$a_n = I_1 \cos(H(t))\{\frac{\lambda}{2L\pi(2n+1)}\sin\frac{2L\pi(2n+1)}{\lambda} + \frac{\lambda}{2L\pi(2n-1)}\sin\frac{2L\pi(2n-1)}{\lambda}\}$$

$$= I_1 \cos(H(t))\{\frac{2}{\pi(2n+1)}(-1)^n + \frac{2}{\pi(2n-1)}(-1)^{n+1}\}$$

$$= 4I_1 \cos(H(t))\frac{(-1)^{n+1}}{(2n+1)(2n-1)\pi}$$

$$b_n = I_1 \sin(H(t))\{\frac{-\lambda}{2L\pi(2n+1)}\sin\frac{2L\pi(2n+1)}{\lambda} + \frac{\lambda}{2L\pi(2n-1)}\sin\frac{2L\pi(2n-1)}{\lambda}\}$$

$$= I_1 \sin(H(t))\{\frac{2}{\pi\,(2n+1)}(-1)^{n+1} + \frac{2}{\pi\,(2n-1)}(-1)^{n+1}\}$$

$$= 4I_1 \sin(H(t))\frac{2n(-1)^{n+1}}{(2n+1)(2n-1)\pi} \tag{A9}$$

$$c_n = \frac{4I_1}{(2n+1)(2n-1)\pi}[\cos^2(H(t)) + 4n^2\sin^2(H(t))]$$

$$= \frac{2I_1}{\pi}[\frac{4n^2+1}{4n^2-1} - \cos 2H(t)] \tag{A10}$$

$$tgh_n = 2n * tg(H(t)),$$

$$Q_n = 2n\ ,\ \ n = 1, 2, 3, \ldots\ldots, +\infty.$$

Many harmonics are included in the Fourier expansion

$$I(x,t) = I_0 + \frac{4I_1}{\pi}\cos(H(t))$$

$$+\sum_{n=1}^{\infty}\ \frac{2I_1}{\pi}[\frac{4n^2+1}{4n^2-1} - \cos 2H(t)]\cos(\frac{n\pi\,x}{L} - h_n(t)) \tag{A11}$$

Suppose $H(t)$ =0 around time t at x=0, then

$$c_n = \frac{2I_1}{\pi}[\frac{2}{4n^2-1}]$$

is independent of time and decreases quickly to 0 as n increases. Therefore,

$$I(x,t) = I_0 + \frac{4I_1}{\pi} + \sum_{n=1}^{\infty}\ \frac{2I_1}{\pi}[\frac{2}{4n^2-1}]\cos(\frac{n\pi\,x}{L} - h_n(t)) \tag{A12}$$

For the n -th harmonic from Eqs.A10 and A7,

$$u_n = \frac{L}{n\pi}\frac{dh_n}{dt} = \frac{\lambda}{2\pi}\frac{dH}{dt} \tag{A13}$$

is independent of n . So an average such as

$$\frac{1}{N}\sum_{n=1}^{N} u_n\ ,\qquad \text{or}\qquad \sum_{n=1}^{N} u_n c_n \,/\, \sum_{n=1}^{N} c_n \tag{A14}$$

over the first N harmonics can be taken as an estimate of the travelling speed .

A-4. M≡2L= $r\lambda$

Here r can be any real number(the case for integer numbers has been discussed above). r >1 means that more than one waves are included in the range [-L, L]. Otherwise, less than 1 wave in the range [-L, L] results in r <1. In this situation,

$$a_0 = 2I_0 + \frac{2I_1}{r\pi}\sin r\pi \cos(H(t))$$

$$a_n = I_1 \cos(H(t))\{\frac{1}{(n+r)\pi}\sin(n+r)\pi + \frac{1}{(n-r)\pi}\sin(n-r)\pi\}$$

$$b_n = I_1 \sin(H(t))\{\frac{-1}{(n+r)\pi}\sin(n+r)\pi + \frac{1}{(n-r)\pi}\sin(n-r)\pi\} \qquad \text{(A15)}$$

Simply increasing $r>1$ can help make c_n independent of time. As r increases, $\frac{1}{(n+r)\pi}$ tends to 0 so that

$$Q_n \to 1$$

$$a_0 \to 2I_0$$

$$a_n \to I_1 \cos(H(t))\{\frac{1}{(n-r)\pi}\sin(n-r)\pi\}$$

$$b_n \to I_1 \sin(H(t))\{\frac{1}{(n-r)\pi}\sin(n-r)\pi\}$$

$$c_n \to I_1 \frac{1}{(n-r)\pi}\sin(n-r)\pi$$

$$h_n \to H(t)$$

$$I(x,t) \to I_0 + \sum_{n=1}^{\infty} I_1 \frac{1}{(n-r)\pi}\sin(n-r)\pi \cos(\frac{n\pi x}{L} - h_n) \qquad \text{(A16)}$$

$$u_n \to \frac{L}{n\pi}\frac{dh_n}{dt} = \frac{r\lambda}{2n\pi}\frac{dH}{dt} \qquad \text{(A17)}$$

Thus, $n \approx r$ is the best for estimating the travelling speed. Amplitude c_n has its maximum at $n \approx r$ so the amplitude-weighted average is preferred for estimating u :

$$\hat{u} = \sum_{n=1}^{N} u_n c_n \,/\, \sum_{n=1}^{N} c_n \qquad \text{(A18)}$$

For $0<r<1$,

$$Q_n = \frac{(n+r)\sin(n-r)\pi - (n-r)\sin(n+r)\pi}{(n+r)\sin(n-r)\pi + (n-r)\sin(n+r)\pi} = \frac{n}{r} \qquad \text{(A19)}$$

Suppose $H(t)$ is small enough at x=0 and c_n is independent of time. Similar to Eq.A13, the phase speed for the n-th harmonic would be approximated by

$$u_n = \frac{L}{n\pi}\frac{dh_n}{dt} = \frac{r\lambda}{2n\pi}Q_n\frac{dH}{dt} = \frac{\lambda}{2\pi}\frac{dH}{dt} \qquad \text{(A20)}$$

which is an estimate of the travelling speed.

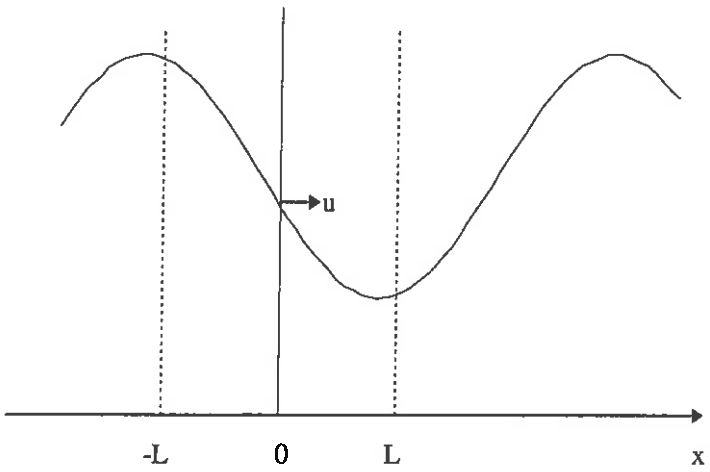

Fig.1 Schematic of an image line

Fig 2a

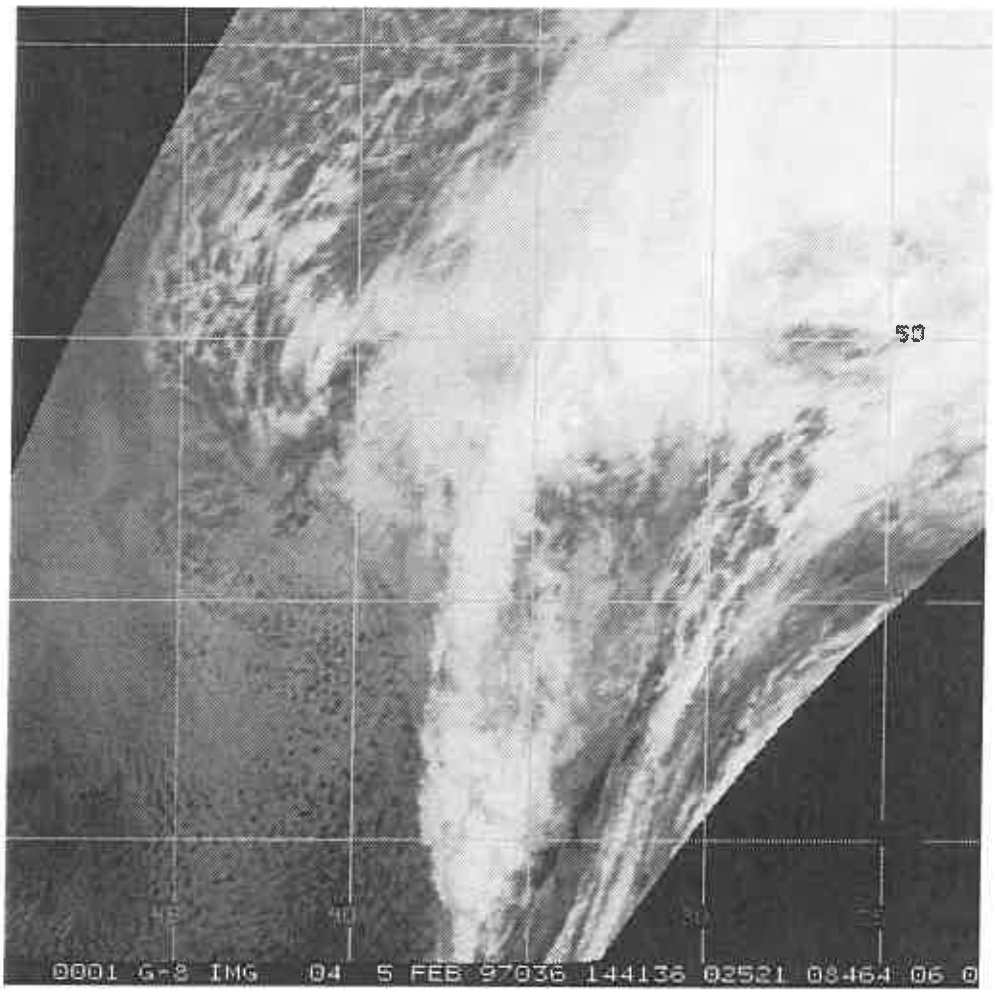

Fig 2b CMW from Fourier Series Analysis of GOES 1-min IR images

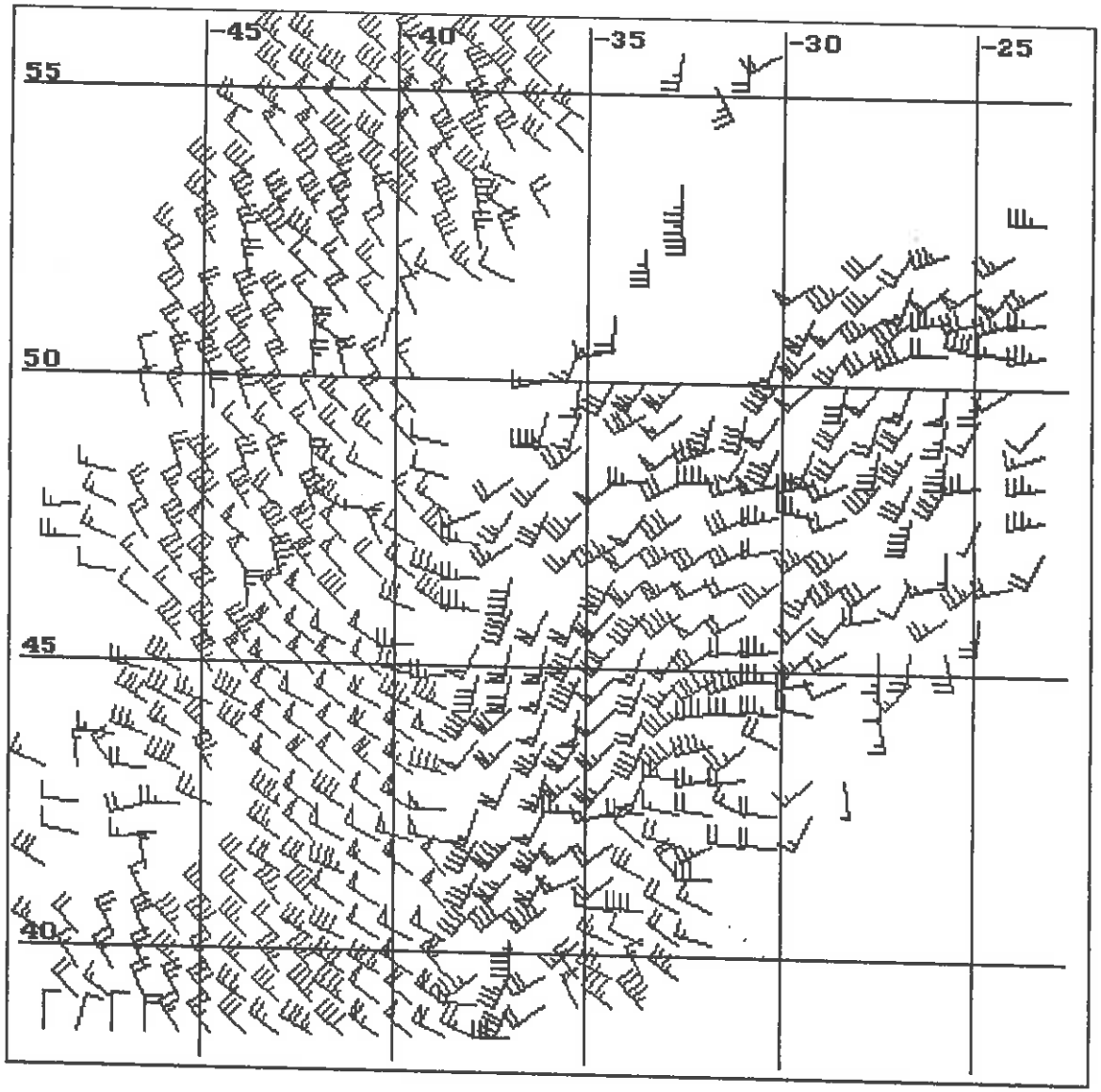

Fig 2b

Fig 2c Standard deviation of CMIN from Fourier Series Analysis

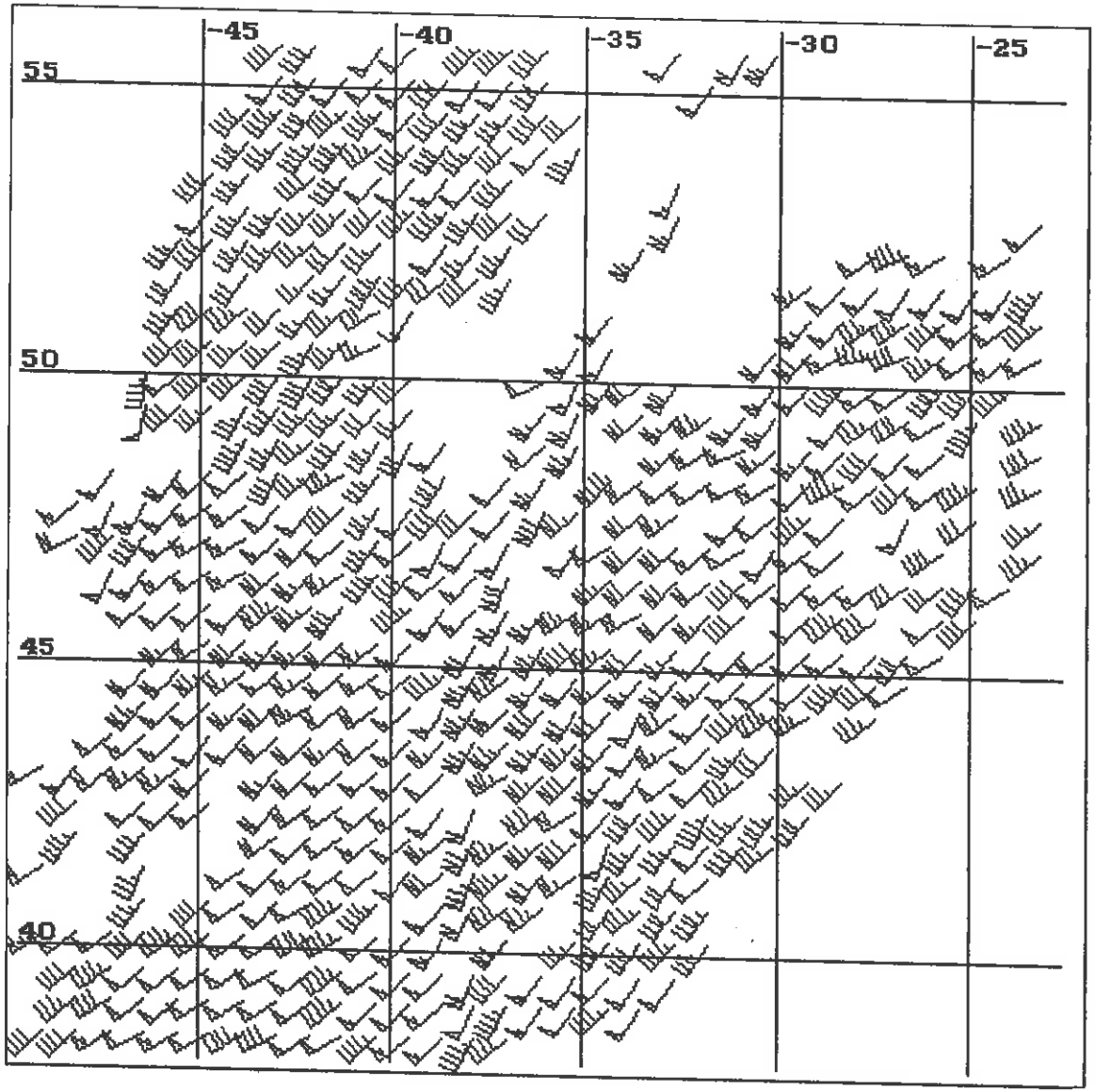

Fig 2c

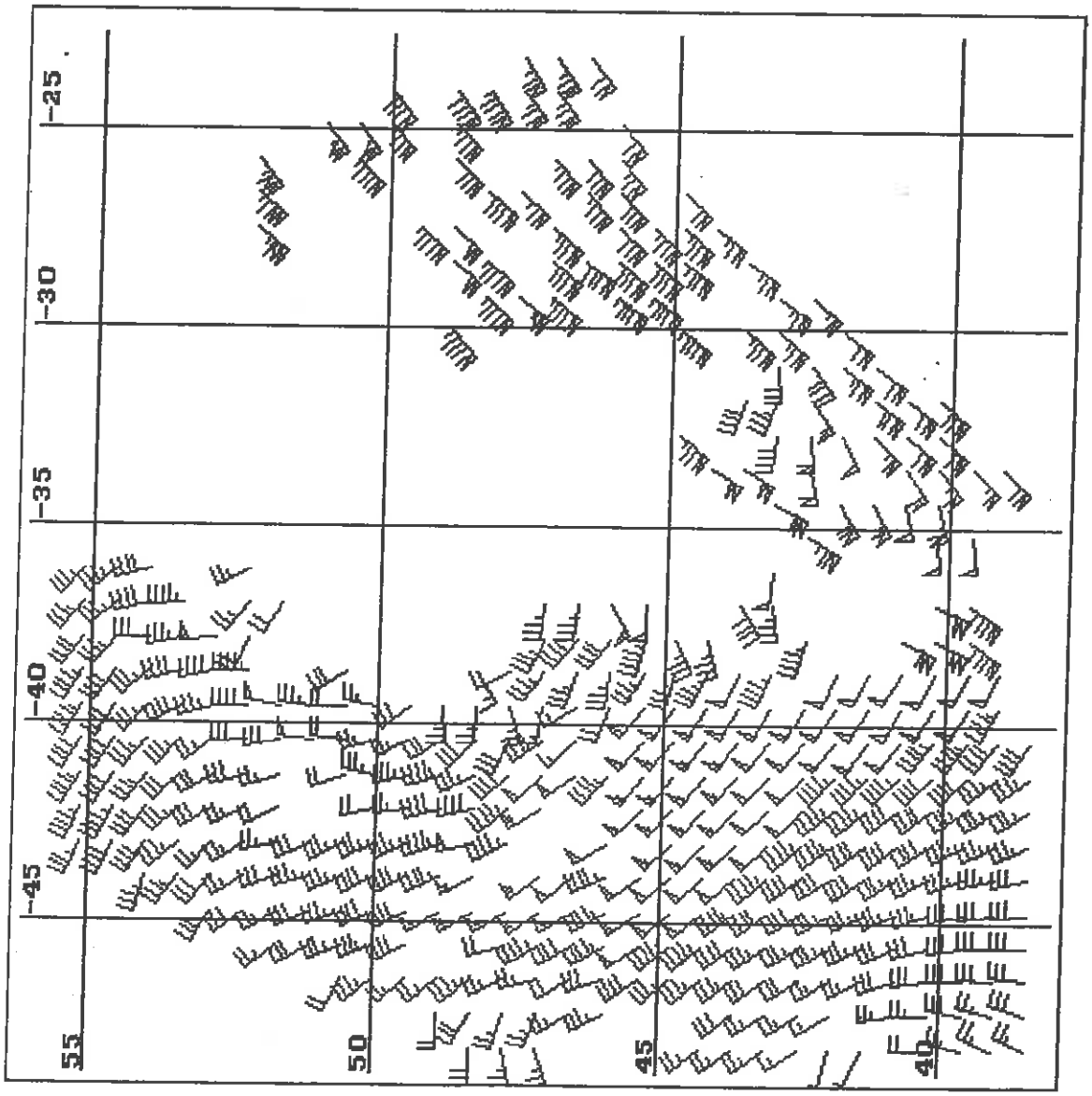

Fig 2d

Fig 2d CMW from Maximum Cross-correlation Analysis of GOES 30-min IR images

CURRENT JCMM INTERNAL REPORTS

This series of JCMM Internal Reports, initiated in 1993, contains unpublished reports and also versions of articles submitted for publication. The complete set of Internal Reports is available from the National Meteorological Library on loan, if required.

1. **Research Strategy and Programme**
   K A Browning et al
   January 1993

2. **The GEWEX Cloud System Study (GCSS)**
   GEWEX Cloud System Science Team
   January 1993

3. **Evolution of a mesoscale upper tropospheric vorticity maximum and comma cloud from a cloud-free two dimensional potential vorticity anomaly**
   K A Browning
   January 1993

4. **The Global Energy and Water Cycle**
   K A Browning
   July 1993

5. **Structure of a midlatitude cyclone before occlusion**
   K A Browning and N Roberts
   July 1993

6. **Development in Systems and Tools for Weather Forecasting**
   K A Browning and G Szejwach
   July 1993

7. **Diagnostic study of a narrow cold frontal rainband and severe winds associated with a stratospheric intrusion**
   K A Browning and R Reynolds
   August 1993

8. **Survey of perceived priority issues in the parametrizations of cloud-related processes in GCMs**
   K A Browning
   September 1993

9. **The Effect of Rain on Longwave Radiation**
   I Dharssi
   September 1993

10. **Physical Cloud Microprocesses - A Description of the Parametrization used in the Large Eddy Model**
    H Swann
    July 1994

11. **An Appreciation of the Meteorological Research of Ernst Kleinschmidt**
A J Thorpe
May 1992

12. **Potential Vorticity of Flow Along the Alps**
A J Thorpe, H Volkert and Dietrich Heimann
August 1992

13. **The Representation of Fronts**
A J Thorpe
January 1993

14. **A Parametrization Scheme for Symmetric Instability: Test for an Idealised Flow**
C S Chan and A J Thorpe
February 1993

15. **The Fronts 92 Experiment: a Quicklook Atlas**
Edited by T D Hewson
November 1993

16. **Frontal wave stability during moist deformation frontogenesis**
Part 1. Linear wave dynamics
C H Bishop and A J Thorpe
May 1993

17. **Frontal wave stability during moist deformation frontogenesis**
Part 2. The suppression of non-linear wave development
C H Bishop and A J Thorpe
May 1993

18. **Gravity waves in sheared ducts**
C Bishop and A J Thorpe
November 1993

19. **Potential Vorticity and the Electrostatics Analogy: Quasi-Geostrophic Theory**
C Bishop and A J Thorpe
November 1993

20. **Recent Advances in the Measurement of Precipitation by Radar**
A J Illingworth - April 1993

21. **Micro-Physique et Givrage. Cloud Microphysics and Aircraft Icing**
A J Illingworth May 1993

22. **Differential Phase Measurements of Precipitation**
M Blackman and A J Illingworth
May 1993

23. **Estimation of Effective Radius of Cloud Particles from the Radar Reflectivity**
N I Fox and A J Illingworth
May 1993

24. **A Simple Method of Dopplerising a Pulsed Magnetron Radar**
A Hau, A J Illingworth and J Eastment
November 1993

25. **Radiation and Polar Lows**
George C Craig
February 1994

26. **Collected preprints submitted to the International Symposium on the Life Cycles of Extratropical Cyclones; Bergen, Norway, 27 June - 1 July 1994**
April 1994

27. **Convective Frontogenesis**
Douglas J Parker and Alan J Thorpe
April 1994

28. **Improved Measurement of the Ice Water Content in Cirrus Using a Total Water Evaporator**
Philip R A Brown and Peter N Francis
April 1994

29. **Mesoscale Effects of a Dry Intrusion within a Vigorous Cyclone**
K A Browning and B W Golding
April 1994

30. **GEWEX Cloud System Study, Science Plan**
May 1994

31. **Parametrization of Momentum Transport by Convectively Generated Gravity Waves**
R Kershaw
February 1995

32. **Mesoscale Modelling Newsletter No 5**
May 1994

33. **Observations of the mesoscale sub-structure in the cold air of a developing frontal cyclone**
K A Browning, S A Clough, C S A Davitt, N M Roberts and T D Hewson
May 1994

34. **Longwave Radiative Forcing of a Simulated Tropical Squall Line**
Imtiaz Dharssi
July 1994

35. **On the nature of the convective circulation at a kata-cold front**
K A Browning
September 1994

36. **Collective preprints of papers submitted to the COST-75 International Seminar on Advanced Weather Radar Systems, Brussels, 20-23 September 1994**
November 1994

37. **Use of satellite imagery to diagnose events leading to frontal thunderstorms: Parts 1 and 11 of a case study**
K A Browning and N M Roberts
November 1994

38. **The role of spaceborne millimetre-wave radar in the global monitoring of ice cloud**
P R A Brown, A J Illingworth, A J Heymsfield, G M McFarquahar, K A Browning and M Gosset
December 1994

39. **Potential Vorticity Inversion**
Michael Ziemianski
October 1994

40. **Theory of mature tropical cyclones; a comparison between Kleinschmidt (1951) and Emanuel (1986)**
Suzanne L Gray
December 1994

41. **Dispersion and removal of pollutants during the passage of an atmospheric frontal System**
N R Gimson
December 1994

42. **The role of snow sublimation in frontogenesis**
D J Parker and A J Thorpe
December 1994

43. **Potential vorticity and the electrostatics Analogy: Ertel- Rossby formulation**
A J Thorpe and C H Bishop
December 1994

44. **Mesoscale aspect of extratropical cyclones: an observational perspective**
K A Browning
January 1995

45. **A Polar Low Outbreak: Evolution and Mesoscale Structures**
T D Hewson, G C Craig and C Claud
February 1995

46. **Generation of near-surface gusts of deep convection**
K Nakamura and R Kershaw
April 1995

47. **Attribution Concepts applied to the Omega Equation**
S A Clough, C S A Davitt and A J Thorpe
June 1995

48. **Parametrization of mixed-phase cloud and precipitation**
Susan P Ballard and M Gerard Hutchinson
June 1995

49. **Short-range forecasting of stratocumulus: Initialization Prediction**
Susan Ballard, Simon D Jackson and B Macpherson
June 1995

50. **Contributions of the JCMM/Dept of Meteorology Radar Group to the 27th AMS Radar Meteorology Conference, Vail October 1995**
June 1995

51. **Cold Pools in Shear**
Douglas J Parker
September 1995

52. **High-resolution analysis of frontal fracture**
K A Browning, S P Ballard and C S A Davitt
September 1995

53. **The Albedo of Broken Cloud Fields: Calculations using a modified two stream radiation code**
Imtiaz Dharssi and Roy Kershaw
October 1995

54. **Parametrization of momentum transport by convection. I: Theory and cloud modelling results**
P Kershaw and D Gregory
November 1995

55. **Variation of frontal structure along a cold front**
K A Browning and N M Roberts
November 1995

56. **Secondary Frontal Waves**
Douglas Parker
December 1995

57. **Objective Fronts**
T D Hewson
March 1996

58. **Mesoscale analysis of the activation of a cold front during cyclogenesis**
K A Browning, N M Roberts and A J Illingworth
June 1996

59. **Investigation of Different Representations of Rain in a 1-d Evaporation Model**
H Swann
May 1996

60. **Parametrization of diabatic processes in the inversion of the omega-equation**
M Athanassiadou and A J Thorpe

61. **The Role of the Environmental Flow in the Development of Secondary Frontal Cyclones**
I A Renfrew, A J Thorpe and A Joly
June 1996

62. **Consequences of the geostrophic momentum approximation on barotropic instability**
S Malardel, A J Thorpe and A Joly
June 1996

63. **Contributions to the AMS/RMS Conference on Mesoscale Processes**
Reading, 9-13 September 1996

64. **Vorticity and Potential Vorticity in Stratified Flows Interacting with an Isolated Obstacle**
Jorge A Gutierrez and A J Thorpe
September 1996

65. **Triple Point Development: Two Case Studies**
Douglas Parker
September 1996

66. **Radar observations of wind-shear splitting within evolving atmospheric Kelvin-Helmholtz billows**
D Chapman and K A Browning
April 1997

67. **Cold Frontal Structure derived from radar wind profilers**
K A Browning, D Jerrett, J Nash, T Oakley, N M Roberts
May 1997

68. **The dry intrusion and its effect on the frontal, cloud and precipitation structure of extratropical cyclones**
K A Browning - Text of invited special lecture at the Spring Conference of the Meteorological Society of Japan, University of Tsukuba, 22 May 1997

69. **Met. Office Unified Model data, diagnostic graphics programs, and other observational data available from the JCMM through the aegis of the Universities Weather Research Network UWERN.** Plus supplement.
Peter Panagi and Ed Dicks
June 1997

70. **Contributions of the JCMM/Dept of Meteorology Radar Group to 28th AMS Radar Meteorology Conference.** Austin, Texas, September 1997

71. **Sensitivity of short-range weather forecasts to local potential vorticity modifications**
Meral Demirtas and Alan Thorpe
July 1997

72. **Objective identification of frontal wave cyclones**
T D Hewson
August 1997

73. **Attribution and its application to mesoscale structure associated with tropopause folds**
A J Thorpe
September 1997

74. **The Role of the Environmental Flow in the Development of Secondary Frontal Cyclones**
Ian A Renfrew, Alan J Thorpe and Craig H Bishop
September 1997

75. **Potential Vorticity: A short history of its definitions and uses**
Alan J Thorpe and Hans Volkert
September 1997

76. **Superposing Semi-Geostrophic Potential Vorticity Anomalies**
H R Birkett and A J Thorpe
September 1997

77. **Short period forecasting of catchment-scale precipitation. Part 1: the role of Numerical Weather Prediction**
M A Pedder, M Haile and A J Thorpe
September 1997

78. **Verification of the Tracking Technique Used in an Experimental Cloud Motion Wind Inferring System**
Z Wang, K A Browning and G A Kelly
October 1997

79. **A Preliminary Study of Fourier Series Analysis for Cloud Tracking with GOES High Temporal Resolution Images**
Z Wang
October 1997

Met Office Joint Centre for Mesoscale Meteorology Department of Meteorology
University of Reading PO Box 243 Reading RG6 6BB United Kingdom
Tel: +44 (0)118 931 8425 Fax: +44 (0)118 931 8791
www.metoffice.com